Simultaneous ground-based observations of a large quasi 26-day wave from three different measurement sites in northern mid-latitudes

Christoph Kalicinsky[1], Sandra Wallis[2], Lukas Depenthal[2], Christoph G. Hoffmann[2], Anna Lange[2], and Christian von Savigny[2]

[1]Institute for Atmospheric and Environmental Research, University of Wuppertal, Germany
[2]Institute of Physics, University of Greifswald, Germany

Correspondence: Christoph Kalicinsky (kalicins@uni-wuppertal.de)

Abstract. We present simultaneous observations of a remarkable planetary wave event in mesospheric temperature observed by three different ground-based mid-latitude OH spectrometers at stations in Germany (Greifswald (54°N, 13°E), Wuppertal (51°N, 7°E), and Hohenpeißenberg (48°N, 11°E)) during boreal winter 2016/2017. Additionally, temperature profile observations with the satellite instruments SABER/TIMED and MLS/Aura are used for supporting information on the global distribution of the wave event.

The observed wave had a period of about 26 days and an amplitude of partly up to about 20 K. The satellite temperature observations confirmed that the wave signature exhibited all the characteristics of the well known Rossby (1,4) normal mode oscillation. To the best of our knowledge this is the first study reporting on such a strong Rossby (1,4) wave in the middle atmosphere of the Northern Hemisphere. The wave signature was also identified in atomic oxygen mixing ratios in the mesopause region and lower thermosphere observed with SABER illustrating the importance of such wave events not only for the temperature distribution but also for the temporal variation of trace-gas distributions.

1 Introduction

Planetary waves are large-scale phenomena that play a crucial role in the global circulation by transporting momentum from lower altitudes upward (e.g. Salby, 1984; Andrews et al, 1987; Volland, 1988). They are typically generated in the lower atmosphere and can propagate vertically, reaching also the mesosphere – lower thermosphere (MLT) region (50 km - 110 km) under certain conditions (e.g. Holton, 1984; Laštovička, 1997; Smith, 2003; Sassi et al., 2012). Ground-based observations are known since decades to be particularly well suited for detecting such waves in the MLT region, employing a variety of techniques to monitor atmospheric parameters such as wind, temperature, and airglow, and they reveal periodicities that span from a few days to several weeks ~~(e.g. ?Yoshida et al., 1999; Bittner et al., 2000; ?; ?; ?; Espy et al., 2005; French et al., 2005; ?; ?; Stockwell et al., 2007;~~ (e.g. Yoshida et al., 1999; Bittner et al., 2000; Espy et al., 2005; French et al., 2005; Stockwell et al., 2007; López-González et al., 2009; D . Within this broad spectrum, certain periodic fluctuations can be attributed to specific Rossby-wave modes, which, although modulated by the background wind field, emerge at relatively well-defined periods when typical background winds are present

(e.g. Kasahara, 1980; Salby, 1981a, b). An observation of a large event with a period of about 28 days reported from an Antarctic station by Zhao et al. (2019) was interpreted as being associated with the Rossby-wave (1,4) mode, reinforcing the link between observed periodicities and underlying wave dynamics. Observations from the GRIPS instrument at the Wuppertal station have demonstrated the capability to also capture such wave events, and a previous analysis showed that a substantial proportion of detections fell within the 25- to 30-day period range (Kalicinsky et al., 2026). In the present study we extend this line of investigation by conducting a detailed analysis of one event within the same period band, incorporating additional ground-based stations and satellite observations to provide a more comprehensive view.

The paper first describes the instruments and datasets employed in section 2, then presents the analysis of a specific winter 2016/17 event in section 3, followed by a discussion of the results and their possible origin in section 4, and finally offers a summary and conclusions.

2 Measurement data

2.1 OH*(3,1) rotational temperature observations

OH*(3,1) rotational temperatures in the mesopause region have been observed from the ground using GRIPS (GRound-based Infrared P-branch Spectrometer) instruments for several decades. The instruments measure three OH*(3,1) P-branch lines – $P_1(2)$, $P_1(3)$, and $P_1(4)$ – in the near-infrared spectral range of 1.524 to 1.543 μm during night and cloud free conditions. The emission layer of excited hydroxyl molecules resides at approximately 87 km altitude with a thickness of about 9 km (Baker and Stair, 1988; Oberheide et al., 2006), but it can vary on different time scales (e.g. von Savigny, 2015; García-Comas et al., 2017). Rotational temperatures are then derived from the relative intensities of the three lines (see Bittner et al., 2000, and references therein) and these temperatures closely approximate kinetic temperatures in the mesopause region, particularly for the (3,1) vibrational band (Noll et al., 2015).

We use three different instruments located at the measurement sites Greifswald (54°N, 13°E), Wuppertal (51°N, 7°E), and Hohenpeißenberg (48°N, 11°E) in Germany (see Fig. 1). The measurements in Wuppertal started in the early 1980s, with continuous measurements since summer 1987. Two instruments conducted these measurements. GRIPS-II, a Czerny-Turner spectrometer with a liquid-nitrogen-cooled Ge detector (see Bittner et al., 2002, for a detailed instrument description), provided data until a detector failure in mid-2011. A new instrument was operated alongside GRIPS-II from early to mid-2011, yielding simultaneous measurements that revealed no significant differences between the systems. The new instrument, featuring similar optical properties but a thermoelectrically cooled InGaAs detector, faced technical issues causing data gaps in 2012 and 2013. After some final reconstructions the instrument called GRIPS-N has run reliably since early 2014 (Kalicinsky et al., 2016, 2024).

The measurements in Hohenpeißenberg were done by GRIPS-I. This instrument is an Ebert–Fastie spectrometer with a liquid-nitrogen-cooled Ge detector (see Bittner et al., 2002, for a detailed instrument description). GRIPS-I started its operation in Hohenpeißenberg end of 2003 and the measurement time series ended in mid 2017 due to a final detector failure.

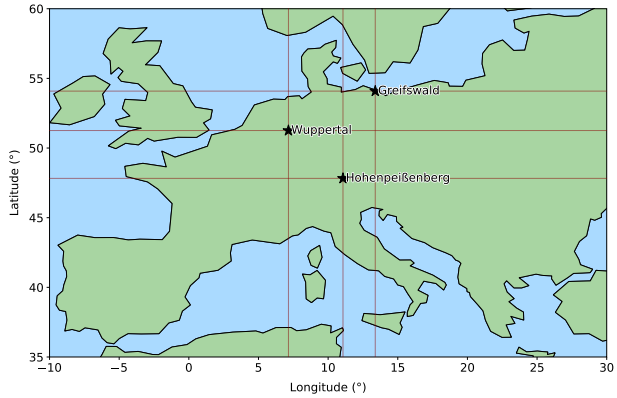

Figure 1. Geographical position of the three GRIPS instruments in Greifswald, Wuppertal, and Hohenpeißenberg.

The observations in Greifswald are performed using an instrument largely identical in construction to the GRIPS 6 spectrometer described in Schmidt et al. (2013). The spectrometer in Greifswald has been operated continuously since 2015, with a single change in observation direction to the zenith in 2022. During the period relevant for the current analysis, the elevation angle was about 40°, so that the OH layer was observed roughly 100 km west of Greifswald.

The time resolution is best in Greifswald and worst in Hohenpeißenberg, because of the shorter and longer integration time (15s vs 270s), respectively. Due to the longest integration time in Hohenpeißenberg, the possibility to encounter cloud influences within a single spectrum is enhanced. Thus, data gaps because of clouds are more frequently observed in Hohenpeißenberg than in Greifswald with Wuppertal (integration time 210s) being in between.

The OH*(3,1) rotational temperatures exhibit a clear seasonal behaviour with lower temperatures in summer and higher temperatures in winter. This seasonal behaviour can be approximated via least-squares fitting of a model incorporating an annual, a semi-annual, and a ter-annual cycle:

$$T(t) = T_0 + \sum_{i=1}^{3} A_i \cdot \sin\left(\frac{2 \cdot \pi \cdot i}{365.25}(t + \phi_i)\right), \tag{1}$$

where t denotes the time in days, T_0 the annual mean temperature, and A_i, ϕ_i are amplitudes and phases of the sinusoids. Several previous studies have utilised this method and it proved to be a good concept (e.g. Bittner et al., 2000; Offermann et al., 2010; Perminov et al., 2014; Kalicinsky et al., 2016, 2024). The residual temperatures that will be analysed in this study are the difference of the measurements and the seasonal fit according to Eq. 1. As we analysed the winter 2016/2017 the fit was calculated from 1 July 2016, to 30 June 2017.

2.2 SABER observations

The Sounding of the Atmosphere using Broadband Emission Radiometry (SABER) instrument is an infrared limb radiometer positioned on the Thermosphere-Ionosphere-Mesosphere Energetics and Dynamics (TIMED) satellite. It started its scientific operation on 22 January 2002 and is active since. TIMED orbits the Earth in a non-sun-synchronous orbit (Russell III et al.,

1999; Esplin et al., 2023). For the current study, SABER Version 2.0 temperature and atomic oxygen profile measurements with a vertical resolution of about 2 km were used (Russell III et al., 1999). Level 2A data was interpolated onto a regular 2 km geometric height grid and daily averaged in the region 48°N to 57°N and 2°W to 28°E to compare it to temperature data sets over Greifswald (54°N, 13°E) and Wuppertal (51°N, 7°E). We restrict these direct comparisons to the two mentioned stations, as the number of data gaps is less compared to Hohenpeißenberg (see Sect. 2.1). Additionally, the SABER temperatures were also daily binned onto a global geographical grid with 5° latitude bins and 30° longitude bins.

2.3 MLS observations

Global temperature data was also used from the Earth Observing System Microwave Limb Sounder (MLS) that uses limb geometry to observe thermal emissions centered near 118, 190, 240 and 640 GHz as well as 2.5 THz. The instrument is located onboard the Aura satellite that performs a sun-synchronous orbit allowing latitude coverage between 82°N to 82°S. MLS started its scientific observations on August 13, 2004 (Waters et al., 2006). This study uses the Level 2 Version 5 temperature product that has an approximate bias with respect to SABER temperatures of +1 K to -5 K between 1 hPa and 0.1 hPa (ca. 50 km - 65 km), 0 K to -3 K between 0.1 hPa and 0.01 hPa (65 km - 80 km) and -10 K at 0.001 hPa (ca. 95 km). The vertical resolution of MLS temperature profiles is 7 – 8 km at 1 to 0.1 hPa, 11 km at 0.01 hPa and 12 km between 0.0001 to 0.0002 hPa (ca. 105 km - 110 km) (Livesey et al., 2022).

The temperature and geopotential height data used in this work were analysed according to the data documentation of Livesey et al. (2022). Only temperature profiles between a pressure range of 261 to 0.00046 hPa were used. Furthermore, the estimated precision of these profiles was required to be a positive number (to exclude data that is strongly impacted by the a priori information) and the status field (a quality metric provided for every profile containing a variety of flags) an even number. We only considered profiles with a data quality greater than 0.2 at 83 hPa and lower pressure levels, and a quality greater than 0.9 at 100 hPa or larger. The convergence field (describing how the fit of the radiances by the retrieval algorithm compares to the expected fit) needed to be less than 1.03 and we omitted profiles between 261 to 100 hPa with an ice water content larger than 0.005 g/m^3 (at 215 hPa) to reduce the interference of clouds. The data was averaged for a global grid with 5° latitude bins and 30° longitude bins to investigate large scale wave patterns.

MLS geopotential height H is used to interpolate the MLS temperatures from a pressure grid to geometric altitudes z using the equation given by Guinn and Mosher (2015):

$$z = \frac{r \cdot H}{r - H} \tag{2}$$

Here, r is the mean Earth radius, set to 6371000 m.

3 Results

3.1 Ground-based observations of the wave event

The wave was simultaneously observed at three independent ground-based stations during the winter of 2016/2017. Pronounced temperature fluctuations are evident in the temperature residuals at all sites (see black curves in Fig. 2). The red curves in Fig. 2 additionally show fits of single sinusoids to the residual temperatures to illustrate the periodic behaviour. The determined amplitudes of the fits represent the mean amplitude of each fluctuation over the duration of the event. Within the interval of interest, the mean period is approximately 25 days at Hohenpeißenberg and Greifswald, and about 27 days at Wuppertal. The corresponding moving Lomb–Scargle periodograms (LSP) (see Kalicinsky et al., 2020, 2024, for a description of the moving LSP) of ~~these~~ the temperature residuals are presented in Fig. 3, where black contours mark regions of statistically significant spectral power. The significance is evaluated by use of the false alarm probability (FAP) that gives the probability that an observed flucutation is caused by chance, e.g. due to noise (see Kalicinsky et al., 2020, 2024, for more details). Obviously, the centre of the wave event at all three sites shows statistically significant results. Because of the ~~increased~~ larger amplitude at the station in Greifswald and the increased temporal coverage of the data due to weather conditions, the area of significant results is larger for Greifswald. Besides this systematic increase in amplitude of the flucuation with latitude, where the station ~~farest~~ farthest north shows the largest amplitude, also a distinct temporal amplitude modulation is evident.

This temporal behaviour is most clearly demonstrated by fitting a sinusoidal function to the time series shown in Fig. 2, with the amplitude modulation parameterized by a Lorentzian-shaped envelope of the form:

$$\frac{A_{max}}{(1+(\frac{(t-t_0)}{\gamma})^2)}, \tag{3}$$

where A_{max} is the maximum amplitude, t the time, t_0 the centre time, and γ the scale parameter. ~~Within the interval of interest, the mean period is approximately 25 days at Hohenpeißenberg and Greifswald, and about 27 days at Wuppertal. The red curves in Fig. 2 additionally show fits of single sinusoids to the residual temperatures and represent the mean amplitude of each fluctuation over the duration of the event.~~

3.2 Satellite-based observations of the wave event

For comparison with the ground-based OH* rotational temperature measurements and to allow for a more comprehensive interpretation of the unusual dynamical situation during winter 2016/2017, which was the strongest wave event in this period range observed by our ground-based instruments in the last decade, we used mesospheric temperature observations ~~with~~ derived from the MLS instrument as well as with SABER. The left panel of Fig. 4 shows the vertical and time dependence of temperature anomalies based on SABER temperature observations. Here the temperature anomalies were determined by subtracting a 41-day running mean from the SABER observations averaged over the Northern German longitude-latitude domain introduced above. ~~A~~ The value of 41 is a subjective choice here, which is long enough for the mean to not follow the short periodic fluctuations but short enough to resemble the seasonal behaviour. Other values could also be used. Furthermore, a subtraction of a seasonal fit would ~~also~~ be a possible way to obtain residuals, too, but it is omitted here as the exact description of

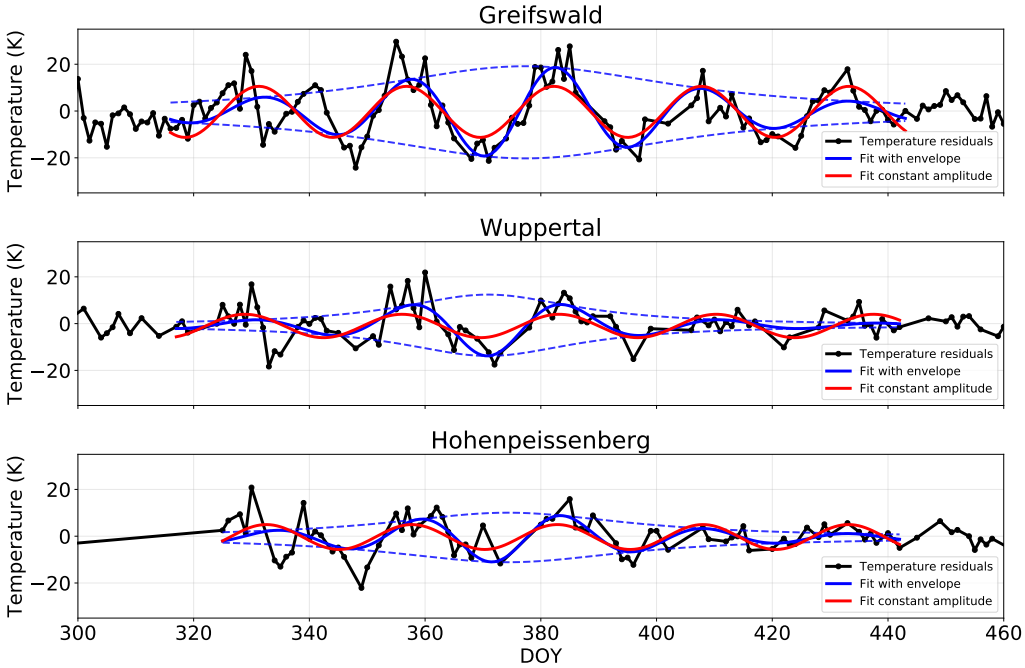

Figure 2. Temperature residuals of the OH*(3,1) rotational temperatures after subtraction of a seasonal fit at Greifswald, Wuppertal, and Hohenpeißenberg (top to bottom) during winter 2016/2017. The residuals are displayed as black curves together with fits to the data. First, a sinusoidal fit with amplitude modulation to the data from DOY 315 to 445 is shown as blue curve. The amplitude modulation follows a Lorentzian function and the envelope is shown as a blue dashed curve separately. Second, a sinusoidal fit with constant amplitude to the data in the same time interval is shown in red.

such a fit describing the seasonal variations differs for each altitude level and depends also on the global region. Note that both daytime and nighttime SABER observations were used. In order to properly compare the temperature anomaly obtained from SABER observations with the temperature anomalies determined from the ground-based observations from Greifswald and Wuppertal, the corresponding SABER temperature profiles were averaged with weighting using the OH*(4-2)/OH*(5-3) volume emission rate (VER) profiles also provided by SABER to obtain OH equivalent temperatures. Before this weighting the VER profiles were shifted downward by 0.75 km in order to consider that the OH centroid emission height increases by about 0.5 km per vibrational level (von Savigny et al., 2012a), because the ground-based instruments measure the OH*(3-1) band, while the SABER VER profiles correspond to the OH*(4-2) and OH*(5-3) bands. The shifted centroid OH emission altitude is shown as the black line in the left panel of Fig. 4. The right panel of Fig. 4 compares the temperature anomalies from the ground-based data sets with the corresponding SABER anomaly. Note here that the anomalies for the OH equivalent temperatures are determined in the same way as for the measured OH*(3,1) rotational temperatures by subtracting a seasonal fit (see Eq. 1). Apparently the overall agreement between the three anomalies is very good and all three data sets exhibit the remarkable quasi-periodic signature with an amplitude typically exceeding 10 K and partly even 20 K.

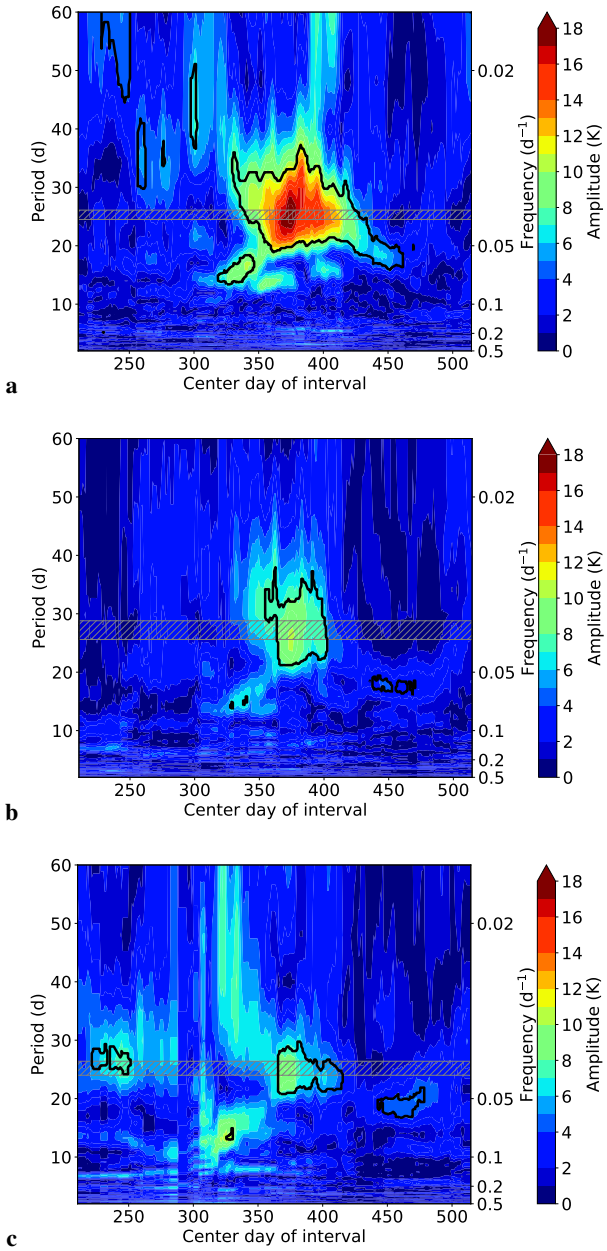

Figure 3. Moving-LSP results for **a** Greifswald, **b** Wuppertal, and **c** Hohenpeißenberg. The results have been obtained with a fixed window size of 60 days. The black lines mark the significant results and the gray hatched areas show the mean period ~~plus minus~~ $\pm$ 2σ determined for the residual temperature time series between DOY 315 and 445 using the sinusoidal fit with fixed period (compare red curve in Fig. 2).

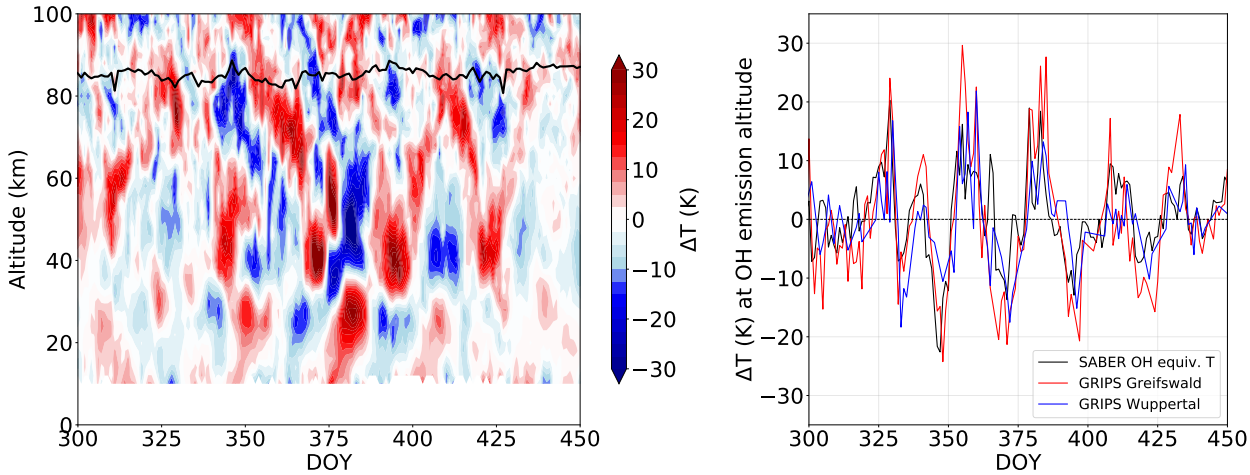

Figure 4. The left panel shows the SABER temperature anomalies for day and night time measurements in the latitude/longitude region 48°N – 57°N and 2°W – 28°E. The centroid altitude of the OH emission layer for the (3,1) band is displayed as a black curve. The right panel shows the time series of the temperature anomalies for the SABER OH equivalent temperatures as a black curve in comparison to the residual temperatures of the OH*(3,1) rotational temperatures observed from Greifswald (red curve) and Wuppertal (blue curve).

4 Discussion

A fluctuation with a period of 25–27 days lies within the range for which the maximum observation frequency for periodic fluctuations of OH*(3,1) rotational temperature was observed in more than 30 years of GRIPS measurements in Wuppertal (Kalicinsky et al., 2024). We hypothesize that a Rossby-wave (1,4) mode can account for a substantial portion of these observations and seek to demonstrate that the event presented in the current study indeed corresponds to such a mode. In the following paragraphs we investigate, whether the unusually large temperature perturbation during winter 2016/2017 discussed here exhibits all the characteristics of a Rossby wave (1,4) mode.

First, a vertical cut through the temperature anomaly field along all longitudes in the latitude band 50°N – 55° N on DOY 371, completing a global transect, is shown in Fig. 5**a** based on SABER ~~(left panel) and MLS (right panel)~~ observations and in Fig. 5**b** based on MLS observations. The Figures reveal a clear zonal wave number 1 structure with antiphased behavior across different altitude regimes. Both satellite instruments concur here, although the MLS measurements exhibit reduced vertical resolution in the upper layers.

Second, horizontal maps of the MLS temperature anomalies at 84 km, 60 km, and 44 km on the same day display the same zonal wave number 1 pattern (see Fig. 6~~**a,b,c**~~**a–c**). These maps are shown for MLS only as this instrument offers superior horizontal coverage but the temperature anomalies for SABER yield qualitatively identical results. Comparing DOY 371 with DOY 384 (see Fig. 6~~**d,e,f**~~**d–f**), which is approximately half a period later, shows the temperature anomaly structures reversing colour (red to blue and vice versa) in many regions, indicating a periodicity of roughly 26 days.

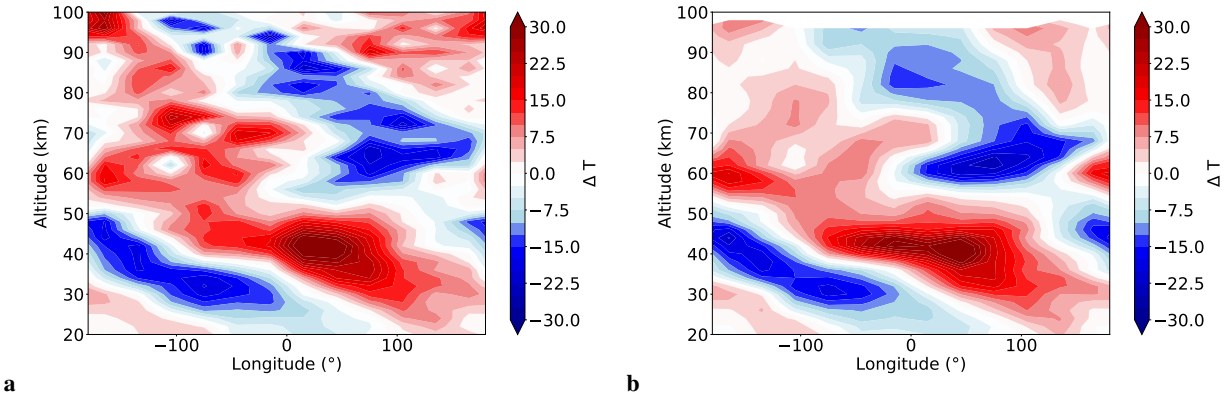

Figure 5. Vertical structure of the SABER (**a**) and MLS (**b**) temperature anomalies against the longitude in the latitude band 50°N-55°N on DOY 371.

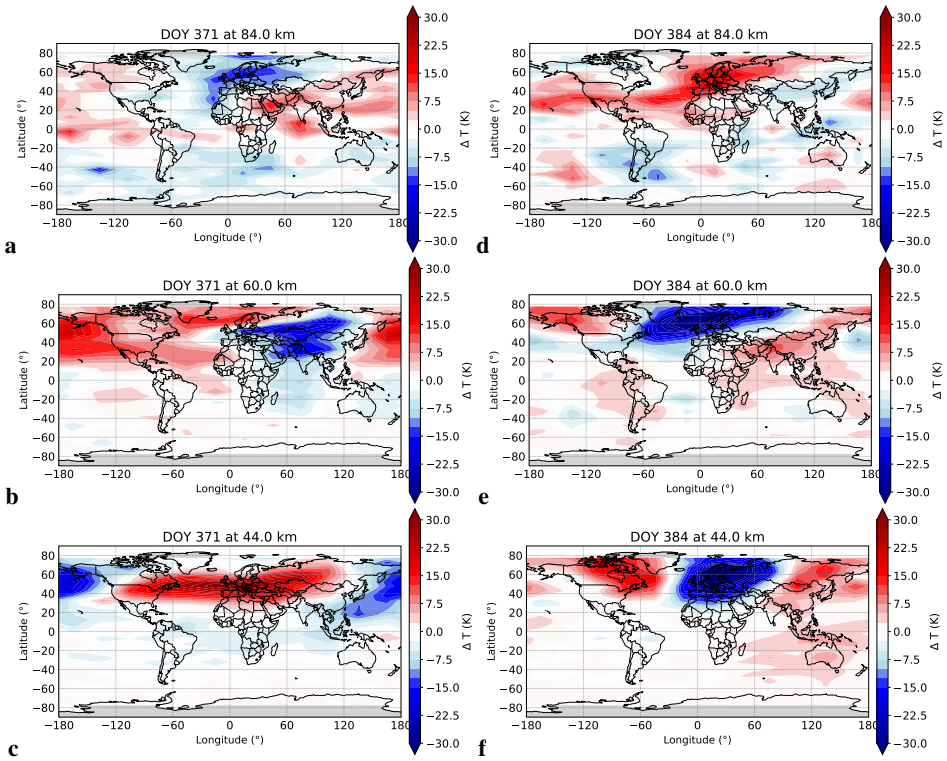

Figure 6. Horizontal maps of the MLS temperature anomalies at DOY 371 at the altitudes **a** 84 km, **b** 60 km, and **c** 44 km and the corresponding temperature anomalies at DOY 384 at the altitudes **d** 84 km, **e** 60 km, and **f** 44 km.

Third, the meridional structure is less apparent in the horizontal maps but becomes discernible in parts of the 84 km height field, likely masked by other fluctuations. Consequently, we fitted sinusoids to the time series for all latitude boxes in the

Northern Hemisphere in the longitude range 0°E – 30° E using both MLS and SABER temperature anomalies at 84 km to improve the determination of the meridional structure. The altitude and the geographical location were chosen according to the ground-based stations. The results for the ~~period, amplitude, and phase~~ periods, amplitudes, and phases are shown in Fig. 7. The mean fitted period is about 26.5 days. The sinusoid phases ~~, expressed as DOY~~ are expressed as the time lag in days of the first ~~positive maximum after DOY 365, cluster around DOY 372 and around DOY 385, form~~ temperature maximum after a reference date, which is DOY 365. These phases cluster around 7 days and around 20 days, forming two groups roughly half a period apart, i.e. the oscillations are antiphased. ~~Phases nearer to DOY 385~~ The amplitues of the fits are all taken as positive values in the first step and then assigned positive or negative according to the phases afterwards. In case of phases nearer to 20 days the amplitudes are assigned positive~~amplitudes, whereas those nearer to DOY 372~~ , whereas the amplitudes for phases nearer to 7 days are assigned negative~~amplitudes~~. The latitudinal amplitude distribution exhibits two pronounced maxima of opposite sign in the Northern Hemisphere, consistent with a Rossby-wave (1,4) mode as proposed by Sassi et al. (2012) for the geopotential height (but the latitudinal distribution for the temperature is the same). The panels of Fig. 7 also show amplitude, phase and period of the wave event determined from the three ground-based OH*(3-1) temperature data sets used here. Apparently, the mean GRIPS amplitudes, periods, and phases agree well with the satellite observations. The latitudes of the GRIPS observations fall within the region of a steep amplitude increase with latitude in the satellite results, which can explain the observed differences at the ground-based measurement sites.

Fourth, the same fitting procedure applied globally to the MLS temperature anomalies at 84 km reproduces the zonal wave number 1 structure in the Northern Hemisphere, with meridional amplitudes of opposite sign near the equator versus high latitudes (see Fig. 8). In the southern hemisphere, a complete sign reversal is evident at large western and eastern longitudes, though it is absent around 0°E. SABER anomalies show a comparable pattern when the sinusoid period is fixed at 26.5 days. Fits allowing a free period yield a noisier but qualitatively identical result, most likely due to data gaps at high northern and southern latitudes.

Collectively, these analyses substantiate that the observed 25–27 day temperature fluctuations are attributable to a Rossby-wave (1,4) mode.

The observed wave exhibits clear implications for other atmospheric constituents, as, e.g. atomic oxygen. Figure 9 illustrates the anomalies of atomic oxygen observed by SABER within the altitude range of 80 km – 100 km in the left panel. The wave event is clearly detectable in atomic oxygen observations. Because the volume mixing ratios of atomic oxygen largely increase with altitude, the absolute effect of the wave intensifies at higher altitudes for the altitude range shown here. In the region of the centroid altitude of the OH layer the absolute effect is relatively small, but still visible. In the right panel of Fig. 9 a comparison between the oxygen anomalies at 84 km (approximately the centroid altitude of the OH layer during winter) and the OH*(3,1) rotational temperatures observed from Greifswald (red curve) and Wuppertal (blue curve) stations is presented. A pronounced correlation can be seen here: relatively higher rotational temperatures, which are indicative of downward motion of air masses and consequent adiabatic heating, coincide with relatively elevated oxygen values. This relationship can be interpreted as the result of downward transport of atomic oxygen from higher altitudes, where its volume mixing ratio is enhanced, whereas upward motions produce the opposite effect.

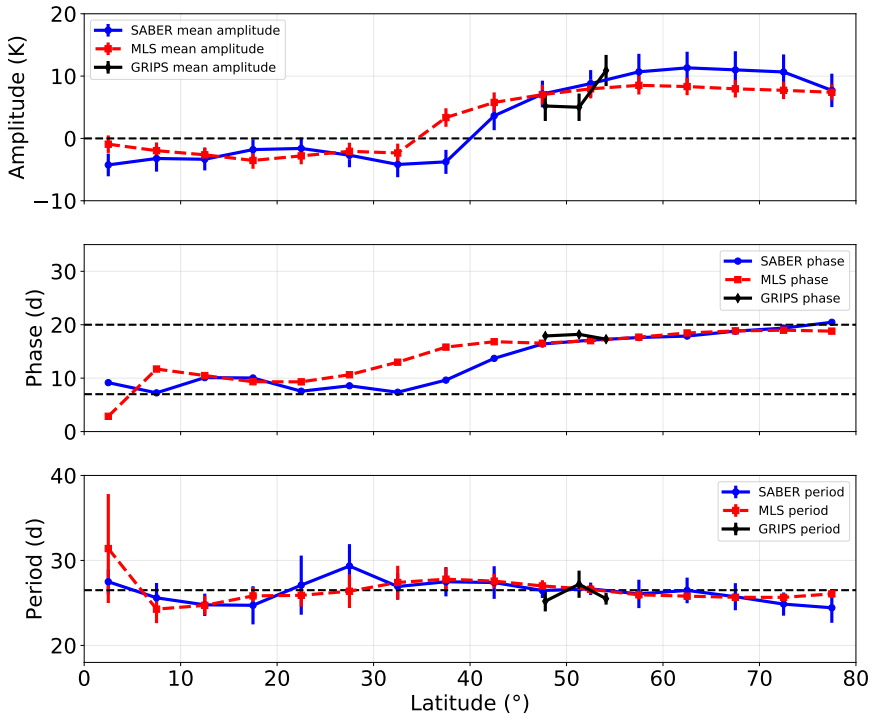

Figure 7. Latitude dependency of the mean amplitude, the phase, and the period of a sinusoidal fit to the data in the time interval DOY 315 to 445. The black curves show the results for the GRIPS OH*(3,1) rotational temperatures, the blue curves for the SABER temperature anomalies at 84 km in the longitude bin 0°E–30°E, and the red curves for the MLS temperature anomalies at the same altitude and longitude bin. The error bars mark the 2-σ uncertainties.

The results presented here possibly also have an effect on investigations of solar 27-day signatures in atmospheric parameters. Solar 27-day signatures have been identified in numerous middle atmospheric parameters including O_3 (Hood, 1986), OH (Shapiro et al., 2012), temperature (including OH* rotational temperature (von Savigny et al., 2012b)) and noctilucent clouds (Robert et al., 2010). Usually, the solar 27-day signatures are identified either using cross-correlation analysis with a solar proxy variable (such as the solar F10.7 cm radio flux or the MgII index) or a superposed epoch analysis with a solar proxy time series as forcing time series. A Rossby wave (1,4) mode signature with amplitudes of 25 K and periods close to 27 days may interfere with the identification of solar 27-day signatures and lead to spurious identifications. The solar 27-day signature in stratospheric and mesospheric temperature has an amplitude of less than 1 K, i.e. much smaller than the possible amplitude of the Rossby wave (1,4) mode. With a superposed epoch analysis – for example – a large number of epochs is required to suppress a 25 K amplitude Rossby wave (1,4) mode signature with a similar period as the sun's rotation. We are not claiming that all previously identified solar 27-day signatures in middle atmospheric parameters are artifacts (see, e.g. Fig. 1 in von Savigny et al. (2012b) or Fig. 3 in Stevens et al. (2026), where connections between temperature and the solar proxy are visible

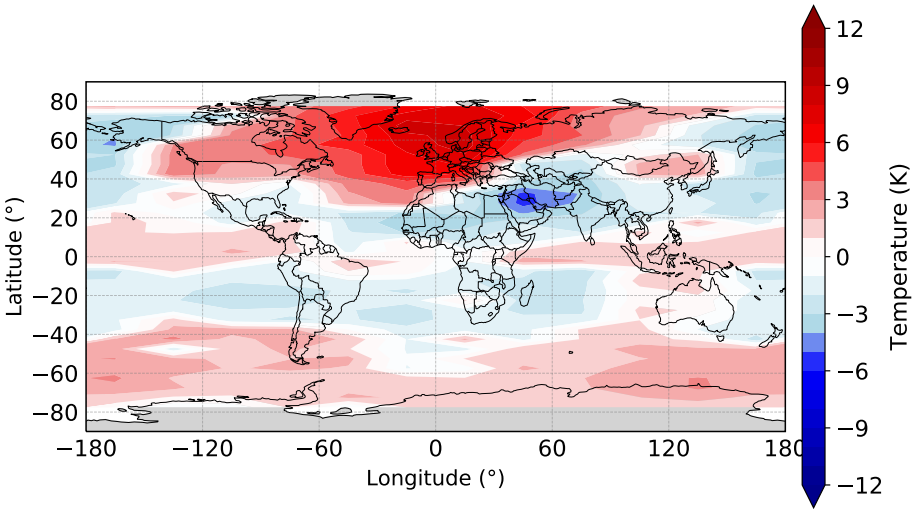

Figure 8. Global distribution of the amplitude of a sinusoidal fit to the MLS temperature anomalies in the time interval DOY 315 to 445. The positive and negative amplitudes are defined according to the phase. For details see text.

to the bare eye). However, future studies should investigate to what extent the detection and quantification of solar 27-day signatures in atmospheric parameters are affected by a Rossby wave (1,4) mode signature and how these different processes can be separated from each other.

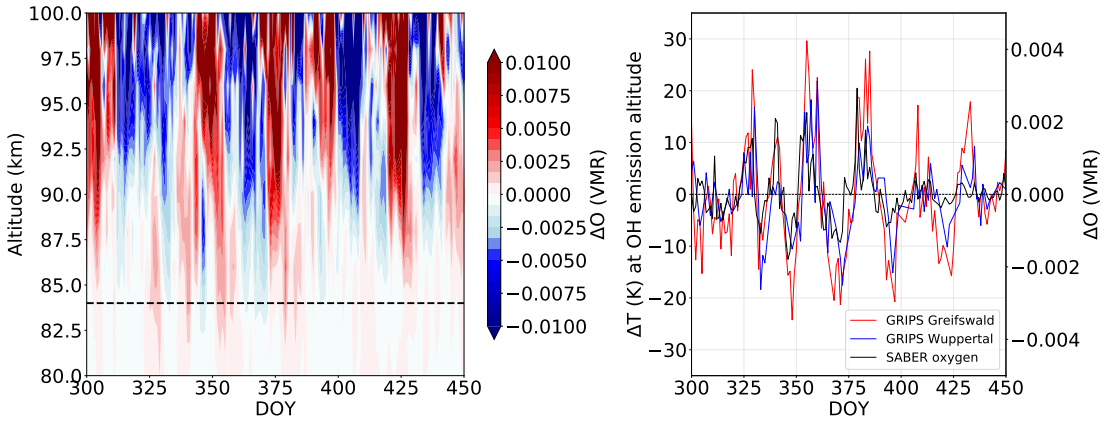

Figure 9. The left panel shows atomic oxygen anomalies derived from SABER observations in the latitude longitude region 48°N – 57°N and 2°W – 28°E. The right panel shows the anomalies at a height level of 84 km (corresponding to the dashed line in the left panel) in comparison to the OH*(3,1) rotational temperatures observed from Greifswald (red curve) and Wuppertal (blue curve).

5 Summary and conclusions

We presented observations of a remarkable planetary wave event in mesospheric temperature during boreal winter 2016/2017 with three different ground-based mid-latitude OH spectrometers and the satellite instruments SABER/TIMED and MLS/Aura. The wave signature had a period of about 26 days, an amplitude of up to about 20 K and covered almost four full cycles. Using the satellite temperature observations we confirmed that the wave signature exhibited all the characteristics of the well known Rossby (1,4) normal mode oscillation. Overall, we found very good agreement between the wave signature in temperatures retrieved from the ground-based and the satellite measurements. To the best of our knowledge this is the first study reporting on such a strong Rossby (1,4) wave in the middle atmosphere of the Northern Hemisphere. The wave signature was also identified in atomic oxygen mixing ratios in the mesopause region observed with SABER and can be expected to be present in other chemical species as well. Further research should clarify the impact of the Rossby (1,4) wave on investigations of solar 27-day signatures in middle atmospheric parameters.

Code availability. TEXT

Data availability. The MLS data is publicly available on https://disc.gsfc.nasa.gov/datasets. SABER data can be downloaded from https://saber.gats-inc.com/browse_data.php. The OH*(3,1) rotational temperatures derived from the GRIPS measurements in Wuppertal and Hohenpeißenberg can be obtained by request to the corresponding author. The OH*(3,1) rotational temperatures for Greifswald can be obtained upon request from Christoph Hoffmann (christoph.hoffmann@uni-greifswald.de).

Code and data availability. TEXT

Author contributions. CK provided the OH*(3,1) rotational temperatures from Wuppertal and Hohenpeissenberg, LD and CH provided the rotational temperatures from Greifswald. SW has processed the SABER and MLS data for the analysis. The main part of the analysis and the preparation of the figures was performed by CK under intensive discussion with all other authors. All authors contributed to the writing of the manuscript.

Competing interests. The authors declare that they have no competing interests.

Disclaimer. TEXT

Acknowledgements. The research by CK was funded by the Deutsche Forschungsgemeinschaft (DFG, German Research Foundation) — 519284835.

The setup and operation of the OH spectrometer at the University of Greifswald was supported by the University of Greifswald. SW and AL acknowledge support by AIR-MoPSy (Atmospheric Impact on the R-Mode Positioning System), an excellence project of the state of Mecklenburg-Western Pomerania, co-funded by the EU within the EFRE programme 2021 - 2027 – EXF-25-1021.

We greatly acknowledge the work done by Peter Knieling and Wolfgang Steinbrecht for running the instruments in Wuppertal and Hohenpeißenberg, respectively.

References

Andrews, D., Holton, J., and Leovy, C.: Middle atmosphere dynamics, Academic Press, London, 1987.

Baker, D. J., and Stair Jr., A. T.: Rocket measurements of the altitude distributions of the hydroxyl airglow, Phys. Scr., 37, 611, doi:10.1088/0031-8949/37/4/021, 1988.

Bittner, M., Offermann, D., and Graef, H. H.: Mesopause temperature variability above a midlatitude station in Europe, J. Geophys. Res., 105, 2045–2058, doi:10.1029/1999JD900307, 2000.

Bittner, M., Offermann, D., Graef, H. H., Donner, M., and Hamilton, K.: An 18-year time series of OH^* rotational temperatures and middle atmosphere decadal variations, J. Atmos. Sol. Terr. Phys., 64, 1147–1166, doi:10.1016/S1364-6826(02)00065-2, 2002.

Day, K. A., and Mitchell, N. J.: The 5-day wave in the Arctic and Antarctic mesosphere and lower thermosphere, J. Geophys. Res., 115, D01109, doi:10.1029/2009JD012545, 2010.

Day, K. A. and Mitchell, N. J.: The 16-day wave in the Arctic and Antarctic mesosphere and lower thermosphere, Atmos. Chem. Phys., 10, 1461–1472, doi:10.5194/acp-10-1461-2010, 2010

~~Egito, F., Buriti, R. A., Fragoso Medeiros, A., and Takahashi, H.: Ultrafast Kelvin waves in the MLT airglow and wind, and their interaction with the atmospheric tides, Ann. Geophys., 36, 231–241, doi:, 2018.~~

Esplin, R., Mlynczak, M. G., Russell, J., Gordley, L., and the SABER Team: Sounding of the Atmosphere using Broadband Emission Radiometry (SABER): Instrument and science measurement description, Earth and Space Science, 10, doi: , 2023.

~~Espy, P. J., Stegman, J., and Witt, G.: Interannual variations of the quasi-16-day oscillation in the polar summer mesospheric temperature, J. Geophys. Res., 102(D2), 1983–1990, doi:, 1997.~~

Espy, P. J., Hibbins, R. E., Riggin, D. M., and Fritts, D. C.: Mesospheric planetary waves over Antarctica during 2002, Geophys. Res. Lett., 32, L21804, doi:10.1029/2005GL023886, 2005.

French, W. J. R., Burns, G. B., and Espy, P. J.: Anomalous winter hydroxyl temperatures at 69°S during 2002 in a multiyear context, Geophys. Res. Lett., 32, L12818, doi:10.1002/2015JD023327, 2005.

~~French, W. J. R., and Klekociuk, A. R.: Long-term trends in Antarctic winter hydroxyl temperatures, J. Geophys. Res., 116, D00P09, doi:, 2011.~~

García-Comas, M., López-González, M. J., González-Galindo, F., de la Rosa, J.L., López- Puertas, M., Shepherd, M. G., and Shepherd, G. G.: Mesospheric OH layer altitude at mid-latitudes: variability over the Sierra Nevada observatory in Granada, Spain (37°N, 3°W), Ann. Geophys., 35, 1151–1164, doi:10.5194/angeo-35-1151-2017, 2017.

~~Hecht, J. H., Walterscheid, R. L., Gelinas, L. J., Vincent, R. A., Reid, I. M., and Woithe, J. M.: Observations of the phase-locked 2 day wave over the Australian sector using medium-frequency radar and airglow data, J. Geophys. Res., 115, D16115, doi:, 2010.~~

Holton, J. R.: The Generation of Mesospheric Planetary Waves by Zonally Asymmetric Gravity Wave Breaking, J. Atmos. Sci., 41, 3427 – 3430, doi:10.1175/1520-0469(1984)041<3427:TGOMPW>2.0.CO;2, 1984.

~~Höppner, K., and Bittner, M.: Evidence for solar signals in the mesopause temperature variability?, J. Atmos. Sol. Terr. Phys., 69, 431–448, doi:, 2007.~~

Guinn, T. and Mosher, F.: Numerical model derived altimeter correction maps for non-standard atmospheric temperature and pressure, International Journal of Aviation, Aeronautics, and Aerospace, 2, 1–22, doi:,2015.

Hood, L. L.: Coupled Stratospheric Ozone and Temperature Responses to Short-Term Changes in Solar Ultraviolet Flux: An Analysis of Nimbus 7 SBUV and SAMS data, J. Geophys. Res., 91, 5264–5276, https://doi.org/10.1029/JD091iD04p05264, 1986.

Kalicinsky, C., Knieling, P., Koppmann, R., Offermann, D., Steinbrecht, W., and Wintel, J.: Long-term dynamics of OH_* temperatures over central Europe: trends and solar correlations, Atmos. Chem. Phys., 16, 15 033–15 047, doi:10.5194/acp-16-15033-2016, 2016.

Kalicinsky, C., Reisch, R., Knieling, P., and Koppmann, R.: Determination of time-varying periodicities in unequally spaced time series of OH* temperatures using a moving Lomb-Scargle periodogram and a fast calculation of the false alarm probabilities, Atmos. Meas. Tech., 13, 467–477, doi:10.5194/amt-13-467-2020, 2020.

Kalicinsky, C., Kirchhoff, S., Knieling, P., and Zlotos, L. O.: Long-term variations in the mesopause region derived from OH*(3,1) rotational temperature observations at Wuppertal, Germany, from 1988 – 2022, Adv. Space Res., 73, 3398–3407, doi:10.1016/j.asr.2023.08.045, 2024.

Kalicinsky, C., Reisch, R., and Knieling, P.: Ground-based observations of periodic temperature fluctuations in the mesopause region with periods longer than 2 d, Atmos. Chem. Phys., 26, 2531–2544, doi:10.5194/acp-26-2531-2026, 2026.

Kasahara, A.: Effect of zonal flows on the free oscillations of a barotropic atmosphere, J. Atmos. Scien., 37(5), 917–929, doi:10.1175/1520-0469(1980)037<0917:EOZFOT>2.0.CO;2, 1980.

~~P. Kishore, Namboothiri, S. P., Igarashi, K., Gurubaran, S., Sridharan, S., Rajaram, R., and Venkat Ratnam, M.: MF radar observations of 6.5-day wave in the equatorial mesosphere and lower thermosphere, J. Atmos. Sol.-Terr. Phys., 66, doi:, 2004.~~

Laštovička, J.: Observations of tides and planetary waves in the atmosphere-ionosphere system, Adv. Space Res., 20, 1209-1222, doi:10.1016/S0273-1177(97)00774-6, 1997.

Livesey, N., Read, W., Wagner, P., Froidevaux, L., Santee, M., Schwartz, M., Lambert, A., Millán, L., Pumphrey, H., Manney, G., Fuller, R., Jarnot, R., Knosp, B., and Lay, R.: Earth observing system (EOS) aura microwave limb sounder (MLS) verion 5.0x level 2 and 3 data quality and description document, JPL D-105336 Rev. B, 5.0–1.1a, doi: (last access: March 2026), 2022.

López-González, M. J., Rodríguez, E., García-Comas, M., Costa, V., Shepherd, M. G., Shepherd, G. G., Aushev, V. M., and Sargoytchev, S.: Climatology of planetary wave type oscillations with periods of 2–20 days derived from O2 atmospheric and OH(6-2) airglow observations at mid-latitude with SATI, Ann. Geophys., 27, 3645–3662, doi:10.5194/angeo-27-3645-2009, 2009.

~~Luo, Y., Manson, A. H., Meek, C. E., Meyer, C. K., and Forbes, J. F.: The quasi 16-day oscillations in the mesosphere and lower thermosphere at Saskatoon (52°N, 107°W), 1980–1996, J. Geophys. Res., 105(D2), 2125–2138, doi:, 2000.~~

Noll, S., Kausch, W., Kimeswenger, S., Unterguggenberger, S., and Jones, A. M.: OH populations and temperatures from simultaneous spectroscopic observations of 25 bands, Atmos. Chem. Phys., 15, 3647–3669, doi:doi.org/10.5194/acp-15-3647-2015, 2015.

Oberheide, J., Offermann, D., Russell III, J. M., and Mlynczak, M. G.: Intercomparison of kinetic temperature from 15 μm CO_2 limb emissions and OH^*(3,1) rotational temperature in nearly coincident air masses: SABER, GRIPS, Geophys. Res. Lett., 33, L14811, doi:10.1029/2006GL026439, 2006.

Offermann, D., Hoffmann, P., Knieling, P., Koppmann, R., Oberheide, J., and Steinbrecht, W.: Long-term trend and solar cycle variations of mesospheric temperature and dynamics, J. Geophys. Res., 115, D18127, doi:10.1029/2009JD013363, 2010.

Perminov, V. I., Semenov, A. I., Medvedeva, I. V., and Zheleznov, Yu. A.: Variability of mesopause temperature from hydroxyl airglow observations over mid-latitudinal sites, Zvenigorod and Tory, Russia, Adv. Sp. Res., 54, 2511–2517, doi:10.1016/j.asr.2014.01.027, 2014.

Reisin, E. R.: Quasi-two-day wave characteristics in the mesopause region from airglow data measured at El Leoncito (31.8°S, 69.3°W), J. Atmos. Sol.-Terr. Phys., 218, 105613, doi:10.1016/j.jastp.2021.105613, 2021.

Robert, C. E., von Savigny, C., Rahpoe, N., Bovensmann, H., Burrows, J. P., DeLand, M. T., and Schwartz, M. J., First evidence of a 27 day solar signature in noctilucent cloud occurrence frequency, J. Geophys. Res., 115, D00I12, https://doi.org/10.1029/2009JD012359, 2010.

Russell, J. M.III, M. G. Mlynczak, L. L. Gordley, J. Tansock, and R. Esplin, An overview of the SABER experiment and preliminary calibration results, in Proceedings of the SPIE, 44th Annual Meeting, Denver, Colorado, July 18–23 , vol. 3756, pp. 277–288, 1999.

Salby, M. L.: Rossby Normal Modes in Nonuniform Background Configurations. Part I: Simple fields, J. Atmos. Sci., 38, 1803–1826, 1981.

Salby, M. L.: Rossby Normal Modes in Nonuniform Background Configurations. Part II: Equinox and Solstice Conditions, J. Atmos. Sci., 38, 1827–1840, 1981.

Salby, M.: Survey of planetary-scale travelling waves: the state of theory and observation, Rev. Geophys. Space Phys., 22, 209–236, 1984

Sassi, F., Garcia, R. R., and Hoppel, K. W.: Large-scale Rossby normal modes during some recent Northern Hemisphere winters, J. Atmos. Scien., 69(3), 820–839, doi:10.1175/JAS-D-1-0103.1, 2012.

Smith, A. K.: The Origin of Stationary Planetary Waves in the Upper Mesosphere, J. Atmos. Sci., 60, 3033 – 3041, doi:10.1175/1520-0469(2003)060<3033:TOOSPW>2.0.CO;2, 2003.

Schmidt, C., Höppner, K., and Bittner, M.: A ground-based spectrometer equipped with an InGaAs array for routine observations of OH(3-1) rotational temperatures in the mesopause region, Journal of Atmospheric and Solar-Terrestrial Physics, 102, 125–139, doi:10.1016/j.jastp.2013.05.001, 2013.

Shapiro, A. V., Rozanov, E., Shapiro, A. I., Wang, S., Egorova, T., Schmutz, W., and Peter, Th.: Signature of the 27-day solar rotation cycle in mesospheric OH and H_2O observed by the Aura Microwave Limb Sounder, Atmos. Chem. Phys., 12, 3181–3188, https://doi.org/10.5194/acp-12-3181-2012, 2012.

Stevens, M. H., Jones, M., Jr., Evans, J. S., Harding, B. J., Dhadly, M. S., and Immel, T. J.: On the strength of solar forcing in the Earth's thermosphere, Geophys. Res. Lett., 53, e2025GL121012. https://doi.org/10.1029/2025GL121012, 2026.

Stockwell, R. G., Riggin, D. M., French, W. J. R., Burns, G. B., and Murphy, D. J.: Planetary waves and intraseasonal oscillations at Davis, Antarctica, from undersampled time series, J. Geophys. Res., 112, D21107, doi:10.1029/2006JD008034, 2007.

~~Takahashi, H., Buriti, R. A., Gobbi, D., Batista, P. P.: Equatorial planetary wave signatures observed in mesospheric airglow emissions, J. Atmos. Sol.-Terr. Phys., 64, 1263–1272, doi:, 2002.~~

~~Takahashi, H., Lima, L. M., Wrasse, C. M., Abdu, M. A., Batista, I. S., Gobbi, D., Buriti, R. A., and Batista, P. P.: Evidence on 2–4 day oscillations of the equatorial ionosphere h′F and mesospheric airglow emissions, Geophys. Res. Lett., 32, L12102, doi:, 2005.~~

Takahashi, H., Shiokawa, K., Egito, F., Murayama, Y., Kawamura, S., Wrasse, C. M.: Planetary wave induced wind and airglow oscillations in the middle latitude MLT region, J. Atmos. Sol.-Terr. Phys., 98, 97–104, doi:10.1016/j.jastp.2013.03.014, 2013.

Volland, H.: Atmospheric Tidal and Planetary Waves. Kluwer Academic Publishers, Boston, 1988.

von Savigny, C., McDade, I. C., Eichmann, K.-U., and Burrows, J. P.: On the dependence of the OH* Meinel emission altitude on vibrational level: SCIAMACHY observations and model simulations, Atmos. Chem. Phys., 12, 8813–8828, https://doi.org/10.5194/acp-12-8813-2012, 2012a.

von Savigny, C., K.-U. Eichmann, C. E. Robert, J. P. Burrows, and M. Weber, Sensitivity of equatorial mesopause temperatures to the 27-day solar cycle, Geophys. Res. Lett., 39, L21804, doi:10.1029/2012GL053563, 2012b.

von Savigny, C.: Variability of OH(3-1) emission altitude from 2003 to 2011: Long-term stability and universality of the emission rate - altitude relationship, J. Atmos. Sol.-Terr. Physics, 127, 120–128, 2015.

Waters, J., Froidevaux, L., Harwood, R., Jarnot, R., Pickett, H., Read, W., Siegel, P., Cofield, R., Filipiak, M., Flower, D., Holden, J., Lau, G., Livesey, N., Manney, G., Pumphrey, H., Santee, M., Wu, D., Cuddy, D., Lay, R., Loo, M., Perun, V., Schwartz, M., Stek, P., Thurstans, R., Boyles, M., Chandra, K., Chavez, M., Chen, G.-S., Chudasama, B., Dodge, R., Fuller, R., Girard, M., Jiang, J., Jiang, Y., Knosp, B., LaBelle, R., Lam, J., Lee, K., Miller, D., Oswald, J., Patel, N., Pukala, D., Quintero, O., Scaff, D., Van Snyder, W., Tope, M., Wagner, P.,

and Walch, M.: The Earth observing system microwave limb sounder (EOS MLS) on the aura Satellite, IEEE T. Geosci. Remote, 44, 1075–1092, doi: , 2006.

Yoshida, S., Tsuda, T., Shimizu, A., and Nakamura, T.: Seasonal variations of 3.0∼3.8-day ultra-fast Kelvin waves observed with a meteor wind radar and radiosonde in Indonesia, Earth Planet Space, 51, 675–684, doi:10.1186/BF03353225, 1999.

Zhao, Y., Taylor, M. J., Pautet, P.-D., Moffat-Griffin, T., Hervig, M. E., Murphy, D. J., French, W. J. R., Liu, H. L., Pendleton Jr., W. R., and, Russell III, J. M., Investigating an unusually large 28-day oscillation in mesospheric temperature over Antarctica using ground-based and satellite measurements, J. Geophys. Res. Atmospheres, 124, 8576–8593. https://doi.org/10.1029/2019JD030286, 2019.